Applied Catalysis B: Environmental 150–151 (2014) 363–369

Contents lists available at ScienceDirect

Applied Catalysis B: Environmental

journal homepage: www.elsevier.com/locate/apcatb

The development of highly crystalline single-phase $Bi_{20}TiO_{32}$ nanoparticles for light driven oxygen evolution

Wei-Nien Su[a,*], Delele Worku Ayele[b], Vincentius Ochie[b], Chun-Jern Pan[b], Bing-Joe Hwang[b,c,**]

[a] Graduate Institute of Applied Science and Technology, National Taiwan University of Science and Technology, Taipei 106, Taiwan
[b] Department of Chemical Engineering, National Taiwan University of Science and Technology, Taipei 106, Taiwan
[c] National Synchrotron Radiation Research Center, Hsinchu 300, Taiwan

ARTICLE INFO

Article history:
Received 26 September 2013
Received in revised form 8 December 2013
Accepted 11 December 2013
Available online 25 December 2013

Keywords:
Bismuth titanates
Photocatalytic activity
Sol–gel
Oxygen production
Single phase

ABSTRACT

The oxygen-producing photocatalysts play a critical role in the development of the artificial Z-scheme photocatalysis. Bismuth titanates have various complex forms, among which $Bi_{20}TiO_{32}$ could be an ideal oxygen evolution photocatalyst, but one has been suffering from its metastable structure and the complicate preparation. Herein, pure phase $Bi_{20}TiO_{32}$ samples were successfully synthesized by a simple sol–gel method followed by calcination of precursors. The effects of chelating agent, source of Bi and Ti precursor's composition have been studied. By combining bismuth nitrate, titanium isopropoxide, and citric acid, highly crystalline $Bi_{20}TiO_{32}$ was obtained after calcination since citric acid helps the formation of a stable complex in the sol–gel preparation with slow hydrolysis reactions due to highly steric hindrance in titanium isopropoxide. The effect of citric acid to metal ion ratio in this synthesis has been studied and optimized. It was found that only calcinations at 375 °C produced a pure phase while others did not. Here we first reported that pure $Bi_{20}TiO_{32}$ with high crystallinity was obtained with 1:1 ratio of citric acid to metal ions and it showed the highest photocatalytic activity of oxygen evolution under the illumination. The effects of grain size and co-catalyst on $Bi_{20}TiO_{32}$ photocatalytic activity of the as-prepared samples have been studied. More generally, it suggests the incorporation of bismuth into a simple oxide of wide band gap via the simple sol–gel method as a strategy to design photocatalysts with excellent properties.

1. Introduction

Conversion of solar energy to chemical energy by water splitting represents an attractive process to solve the global energy and environmental challenges, as sunlight and water are abundant and renewable. Many efforts have been devoted to the searching of efficient photocatalysts to produce hydrogen and oxygen from water under solar energy in the past few decades [1–6]. So far, only a limited number of semiconductor photocatalysts have been reported capable for overall water splitting [2,7,8], because semiconductor materials with suitable redox potentials and band gap for simultaneous water reduction and oxidation are not commonly available. Thus, most research activities are focused on half reactions, that is, separate water reduction and water oxidation involving sacrificial reagents as electron donors and acceptors, respectively. Compared with hydrogen production from water reduction which requires two electrons, water oxidation for oxygen production is more challenging since it requires four holes for generation of two oxygen–oxygen bonds in one oxygen molecule [9–11].

Compared with hydrogen evolution photocatalysts, the reported active photocatalyst systems for oxygen evolution from water oxidation are much fewer. In general, the energy barrier of photocatalytic water oxidation is much higher than that of photocatalytic water reduction. Nowadays many studies have been conducted to develop new light-driven photocatalysts that utilize solar light efficiently for water oxidation. This includes the modification of TiO_2 [12,13] and the development of new types of photocatalysts such as WO_3 and $BiVO_4$ [14–19].

Among the modified TiO_2-based photocatalysts, a Bi-based oxide such as bismuth titanates catches the attention of researchers due to its excellent electronic and optical properties [20,21]. Bismuth titanates belong to a complicated system including several different phases such as $Bi_2Ti_2O_7$, $Bi_2Ti_4O_{11}$, $Bi_4Ti_3O_{12}$, $Bi_{12}TiO_{20}$, $Bi_{20}TiO_{32}$ and so forth. These phases are formed depending on the chemical compositions and processing conditions [22]. In earlier studies, $Bi_2Ti_2O_7$ and $Bi_4Ti_3O_{12}$ show high photocatalytic

* Corresponding author.
** Corresponding author at: Department of Chemical Engineering National Taiwan University of Science and Technology, Taipei 106, Taiwan.
E-mail addresses: wsu@mail.ntust.edu.tw (W.-N. Su), bjh@mail.ntust.edu.tw (B.-J. Hwang).

0926-3373/$ – see front matter © 2013 Elsevier B.V. All rights reserved.
http://dx.doi.org/10.1016/j.apcatb.2013.12.033

activity under UV irradiation [23,24], while $Bi_{12}TiO_{20}$ exhibits high photocatalytic activity under UV or visible light irradiation for degrading methyl orange [25]. Although $Bi_{20}TiO_{32}$ is a photoactive member of the bismuth titanates family that has the potential to possess the desired qualities of a photocatalyst, the photocatalytic activity of $Bi_{20}TiO_{32}$ for oxygen evolution was seldom studied, because it usually appears as metastable phase, and is difficult to obtain it in single phase and high crystallinity. For example, $Bi_{20}TiO_{32}$ has been found as metastable phase at 375 °C during the synthesis of $Bi_7Ti_4NbO_{21}$ [26]. Similarly, $Bi_{20}TiO_{32}$ exists merely as an impurity component during the formation of $Bi_2Ti_2O_7$ nanocrystals and transformed thoroughly into $Bi_2Ti_2O_7$ phase in 3 min at 550 °C [27,28]. According to the conventional phase diagram of Bi_2O_3–TiO_2 system, $Bi_{20}TiO_{32}$ phase is a metastable phase and could not emerge at a low temperature of 400 °C [29]. These all suggest that it is difficult to synthesize $Bi_{20}TiO_{32}$ nanocrystals, limiting the application for photocatalytic water oxidation, which requires a pure and highly crystalline phase (see Supporting information).

Here in, we first fabricated the crystalline and pure $Bi_{20}TiO_{32}$ nanoparticles successfully by a simple sol–gel method and investigated its photocatalytic activity for oxygen evolution. Sol–gel process is a cheap and low-temperature method that allows the fine control of the product's chemical composition. The properties of the as prepared $Bi_{20}TiO_{32}$ samples have been characterized by XRD, SEM and TEM. The photocatalytic activities for oxygen evolution were studied using silver nitrate as sacrificial agent. The photocatalytic activity of the as prepared $Bi_{20}TiO_{32}$ was further enhanced by the addition of co-catalyst such as iridium oxide as a photo-excited hole trapping and platinum as photo-excited electron trapping to the photocatalyst.

2. Experimental

2.1. Chemicals

Bismuth (III) nitrate pentahydrate [$Bi(NO_3)_3{\cdot}5H_2O$, 98%]; titanium (IV) isopropoxide [$Ti(OCH(CH_3)_2)_4$, 98%]; titanium (IV) n-butoxide [$Ti(O(CH_2)_3CH_3)_4$, 99%]; anhydrous citric acid [$C_6H_8O_7$, 99.5%]; ethylenediaminetetraacetic acid [EDTA, $C_{10}H_{16}N_2O_8$, 99.5%]; chloroplatinic acid hexahydrate [$H_2PtCl_6.6H_2O$, 99.9%]; iridium (III) chloride trihydrate [$IrCl_3{\cdot}3H_2O$, 53–56% Ir); methanol [CH_3OH, 99%]; silver nitrate [$AgNO_3$, 99%] were purchased from Acros Organics, whereas nitric acid [HNO_3, 65%] and NaOH (ACS grade, ≥97.0%) was purchased from Sigma Aldrich.

2.2. Synthesis of photocatalysts

Four different combinations of starting materials were used to synthesize $Bi_{20}TiO_{32}$ in order to find the best combination in term of easiness on starting material handling process, easiness on synthesis process and purity of the final product. These are bismuth nitrate–titanium n-butoxide–EDTA (denoted as system 1); bismuth nitrate–titanium isopropoxide–EDTA (system 2); bismuth nitrate–titanium n-butoxide–citric acid (system 3); and bismuth nitrate–titanium isopropoxide–citric acid (system 4). In a typical synthesis, bismuth nitrate was dissolved in a mixture of nitric acid and water (1:5 volume ratio) with constant stirring at room temperature for 1 h. Titanium (IV) isopropoxide or titanium (IV) n-butoxide was added to the bismuth solution with a specific molar ratio under constant stirring at room temperature for 1 h followed by slowly addition of the chelating agent solution under constant stirring at room temperature. The chelating agent solution (solution of citric acid and EDTA) was prepared by dissolving certain amount of citric acid in de-ionized water under constant stirring at room temperature, while EDTA solution was prepared at 80 °C and pH 8.0 (pH was adjusted by using NaOH) and stirred the solution for 2 h. Concentration of metal ions solution and chelating agent solution were calculated to give final concentration of 2.5 g of $Bi_{20}TiO_{32}$ in 100 ml mixed volume. In this particular study, the effect of chelating agent to total metal ions ratio for 1:1, 2:1 and 3:1 was studied. The final solution containing the metal ions and chelating agent solution was put in reflux condenser and heated at 70 °C for 2 h followed by solvent evaporation at 80 °C in an oil bath under constant stirring. Once all the solvent removed, sticky-gel was formed as the result of hydrolysis and polymerization process. The gel was then dried at 110 °C inside oven for 6 h and then converted in to powders using a mortar and pestle. The powders were calcined in cubic furnace under stagnant air condition at 375 °C and 575 °C (the temperature depends on the TGA profiling result of the precursors) using 5 °C/min heating rate for 6 h.

2.3. Co-catalyst loading

Two different co-catalysts have been used in this study; platinum and iridium (IV) oxide as photo-exited electron trapping co-catalyst and photo-exited hole trapping co-catalyst respectively. Platinum for co-catalyst was loaded by photo-deposition method [30,31] using chloroplatinic acid hexahydrate as starting material. 2 g of the as prepared photocatalyst and chloroplatinic acid hexahydrate was dispersed in 20 ml solvent (methanol and de-ionized water mixture (1:4 volume ratio)). Photo-deposition process was carried out in a Pyrex glass cell with cooling water system for 1 h illumination of light. The platinum loaded photocatalyst were washed and collected via repeated centrifugation process at room temperature. After washing process, the platinum loaded photocatalyst was dried in oven at 110 °C for 6 h followed by heat treatment in cubic furnace under stagnant air condition at 375 °C for 3 h with heating rate of 5 °C/min to obtain $Pt/Bi_{20}TiO_{32}$ product. Iridium (IV) oxide as co-catalyst was loaded by an impregnation method [32,33]. 2 grams of the as prepared photocatalyst and iridium (III) chloride trihydrate were dispersed in 20 ml de-ionized water followed by sonication for 2 h. Then the sample was dried in an oven for 12 h at 110 °C under constant stirring to obtain the $IrO_2/Bi_{20}TiO_{32}$ product. The same heat treatment as platinum loading process was applied after the drying process. When both platinum and iridium oxide as co-catalysts were loaded on the photocatalyst, iridium oxide was first loaded on the photocatalyst by impregnation process and then platinum was loaded by photo-deposition process using the same procedure as described above.

2.4. Characterization of photocatalysts

The TEM images were obtained by using a Philips Tecnai 20 G^2-field emission gun with a maximum acceleration voltage of 200 keV. The morphology of the as prepared sample was obtained using a scanning electron microscopy (SEM) system (JEOL Model JEM-6500F FESEM, Tokyo, Japan). The chemical composition of the photocatalyst was measured by Inductively Coupled Plasma Atomic Emission Spectroscopy (Jobin Yvon 2000-2 ICP-AES). X-ray diffraction (XRD) measurements (Bruker D2 Phaser XRD Machine, Germany) were recorded using a Cu Kα radiation source that was operated at 40 kV and 100 mA with a scan rate of 2°/min and 0.05°/point scanning step. Thermo-Gravimetric Analysis (TGA) was performed by using Diamond TG/DTA PerkinElmer using 900 μL aluminum oxide sample holder. UV–vis spectroscopy analysis was performed by using double-beam spectrophotometer (Jasco V-670). A Mercury-Xenon Arc Lamp Power (500 W, Newport) supply was used as the visible light source using a colored glass filter (cut off 420 nm) while a 400-W mercury arc lamp (HB400X~23 from Sen Lights Corporation, Japan) was used for Ultraviolet light source.

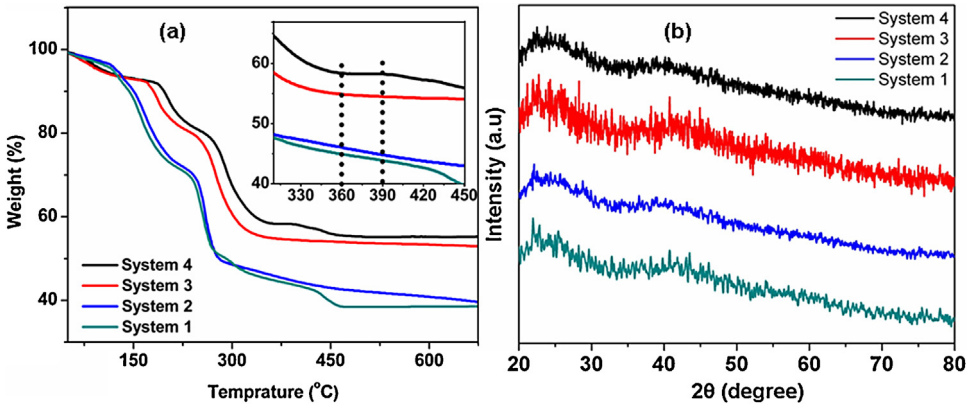

Fig. 1. TGA profile (a) and XRD pattern (b) of metal oxide precursors obtained from different starting material.

The amount of O_2 produced was measured using a 6000 series gas chromatography system ACME 6100 (Younglin Instrument, Porapax N and molecular sieve 5A column, PDHID detector, with helium as the carrier gas).

2.5. Photocatalytic oxygen evolution

The photocatalytic oxygen evolution experiments were carried out in an inner irradiation cell equipped with water cooling system under visible light irradiation. The headspace of the reactor was connected to an inverted burette filled with water at atmospheric pressure, allowing the measurement of the evolved oxygen volume. During the irradiation, the temperature of reaction cells was kept at 25 °C by the circulation of cooling water. In each typical photocatalytic activity test, 0.05 g of photocatalyst was dispersed in 100 ml of 10 mM silver nitrate solution. The suspensions were purged with an argon flow for 30 min before irradiation in order to remove the dissolved oxygen from reaction cell. A 500 W mercury-xenon arc lamp (using a colored glass filter cut off 420 nm) was used as the visible light source to initiate the photocatalytic reaction. The evolved oxygen gas was collected above water through a tube connected to a separate burette and analyzed by a gas chromatograph instrument. The pH of the solution was monitored during photocatalytic oxygen evolution. The stability of photocatalyst for oxygen evolution was verified.

3. Results and discussion

A sol–gel method followed by a calcination process has been employed for the synthesis of pure phase $Bi_{20}TiO_{32}$ for photocatalytic oxygen evolution. The precursors used for the synthesis of $Bi_{20}TiO_{32}$ were obtained using different combinations of starting materials (denoted as systems 1–4). Fig. 1 shows the TGA profiles of the precursors obtained from all systems with corresponding XRD spectra. The TGA profile helps us to understand the properties of the precursors with respect to different temperature in order to determine the suitable combination of starting materials, the calcinations temperature and its effect to the purity of final product. The XRD pattern in Fig. 1(b) shows that the metal oxide precursors obtained in all systems are nearly amorphous. From the ICP-AES data for each metal oxide, the ratio between bismuth to titanium was 20.07, 20.11, 20.12 and 20.06 for system 1, system 2, system 3 and system 4 respectively.

A pure phase $Bi_{20}TiO_{32}$ was obtained after calcination of the metal oxide precursors at different temperatures. The calcination temperature was determined based on the TGA profile of the precursors shown in Fig. 1(a). Only the precursors obtained from system 4 shows a flat line in the region of 365–390 °C while the other system did not show any flat line below 470 °C, suggesting that only system 4 was promising to be used as a precursor to synthesize pure phase $Bi_{20}TiO_{32}$ using a calcination temperature between 365 °C and 390 °C. The calcination temperature, 375 °C was chosen because it is in the middle of the flat region suggesting that it can give enough temperature tolerance in case of temperature fluctuation during calcination process. As a result, the calcination temperature, 375 °C (in the flat region) and 575 °C (out of flat region) were designed for comparison. Thus, the calcination processes for the precursors obtained from different systems were conducted at 375 °C and 575 °C. The ICP-AES result for the product composition between bismuth to titanium after calcination of the precursor obtained from system 1, 2, 3 and 4 at 375 °C and 575 °C are 20.01, 20.07, 20.03, 20.01 and 19.79, 19.86, 19.81 and 19.83 respectively.

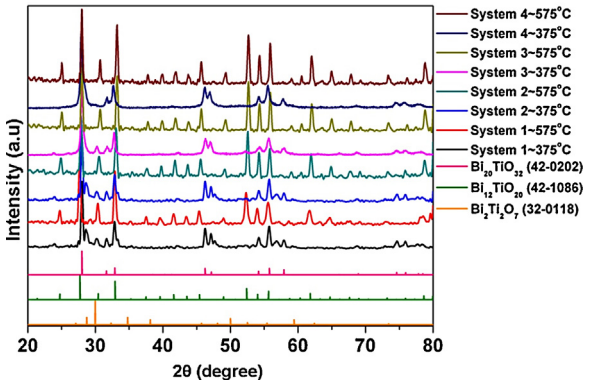

Fig. 2. XRD pattern of the as prepared $Bi_{20}TiO_{32}$ (obtained after calcination of the metal oxide precursors at 375 °C and 575 °C).

XRD patterns shown in Fig. 2 further confirm that the precursor combination in system 4 gives the highest purity of $Bi_{20}TiO_{32}$. We can clearly observe that all peaks of the sample (Fig. 2) obtained from system 4 at 375 °C are identical to the standard $Bi_{20}TiO_{32}$ phase (JCPDS42-0202) and the sharp peaks indicate good crystallinity. Therefore, following experiments in this study, the oxygen evolution photocatalyst $Bi_{20}TiO_{32}$ was synthesized by using the starting material combination in system 4 and 375 °C calcination temperature, unless otherwise stated. The formation of impurities from the precursor combination in systems 1 and 2 in our experiments might resulted from the preparation condition of EDTA solution related to the bismuth nitrate properties and the rate of hydrolysis for different titanium alkoxide precursors. With high hydrolysis rate, titanium alkoxides vigorously react with water producing metal-oxo/hydroxo precipitates which also lead to the formation of impurities [34]. Titanium isopropoxide has lower

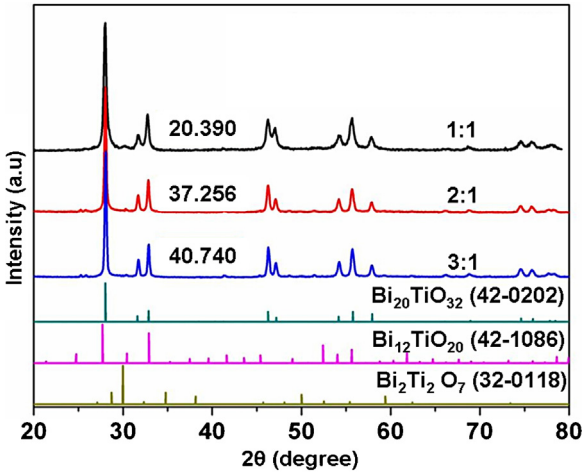

Fig. 3. XRD pattern of the as prepared $Bi_{20}TiO_{32}$ at different citric acid to metal ions ratio (1:1, 2:1, 3:1)) with corresponding JCPDS files for $Bi_{20}TiO_{32}$ (42-0202), $Bi_{12}TiO_{20}$ (42-1086), and $Bi_2Ti_2O_7$ (32-0118).

hydrolysis rate due to steric hindrance effect. This explains that the impurities in system 3 were caused by the higher hydrolysis rate of titanium n-butoxide, when compared to another precursor – titanium isopropoxide in system 4.

In the synthesis of $Bi_{20}TiO_{32}$, the effects of the ratio between chelating agent to the metal ions have been studied. For this purpose, two additional precursors with different citric acid to metal ions ratios (2:1 and 3:1) have been prepared by using the starting material combination in system 4. The citric acid–metal ions solution was then treated following the same procedure as aforementioned. The crystal structure and the grain size of the as prepared $Bi_{20}TiO_{32}$ were compared with the sample prepared by using 1:1 citric acid to metal ions ratio. The XRD spectra (Fig. 3) shows that the increasing crystallinity of the as prepared $Bi_{20}TiO_{32}$ with increasing citric acid to metal ratio may be related to the increasing of metal complex stability in sol–gel precursor. The grain size of $Bi_{20}TiO_{32}$ was calculated from the XRD pattern in Fig. 3 using Scherer equation and equals to 20.390 nm for 1:1 ratio, 37.256 nm for 2:1 ratio and 40.740 nm for 3:1 ratio. This different in grain size for different ratios of chelating agent to metal ion may be due to the formation of larger complex size for higher ratio of citric acid to metal ions eventually leading to the larger cluster of $Bi_{20}TiO_{32}$ in sol–gel precursor and resulted the larger grain size after calcination. Both grain size and crystallinity of the materials significantly affect the photocatalytic activity of oxygen evolution rate.

From the SEM image shown in Fig. 4(a), we can see that the particle size of the sample is around 1.5 μm with some smaller particles around 200 nm attached on them. The particle size of the $Bi_{20}TiO_{32}$ samples from the SEM image is far larger than the average grain size calculated from the Scherer formula and this may account for the particle agglomeration during the preparation process. The TEM images of as prepared $Bi_{20}TiO_{32}$ photocatalyst (Fig. 4(b)) shows that the sample has a good crystallinity with crystal size around 20–30 nm, which is relatively consistent with the XRD results. Fig. 4(c) shows the UV–vis absorbance spectra of the as prepared samples. The products exhibit good absorption in the visible region. The band gap value of the as prepared $Bi_{20}TiO_{32}$ sample was estimated from the UV–vis absorbance spectra and it was approximately around 2.38 eV.

3.1. The photocatalytic activity of the as prepared $Bi_{20}TiO_{32}$ for oxygen evolution

Photocatalytic activity of the as prepared samples for oxygen evolution was performed in silver nitrate aqueous solution where

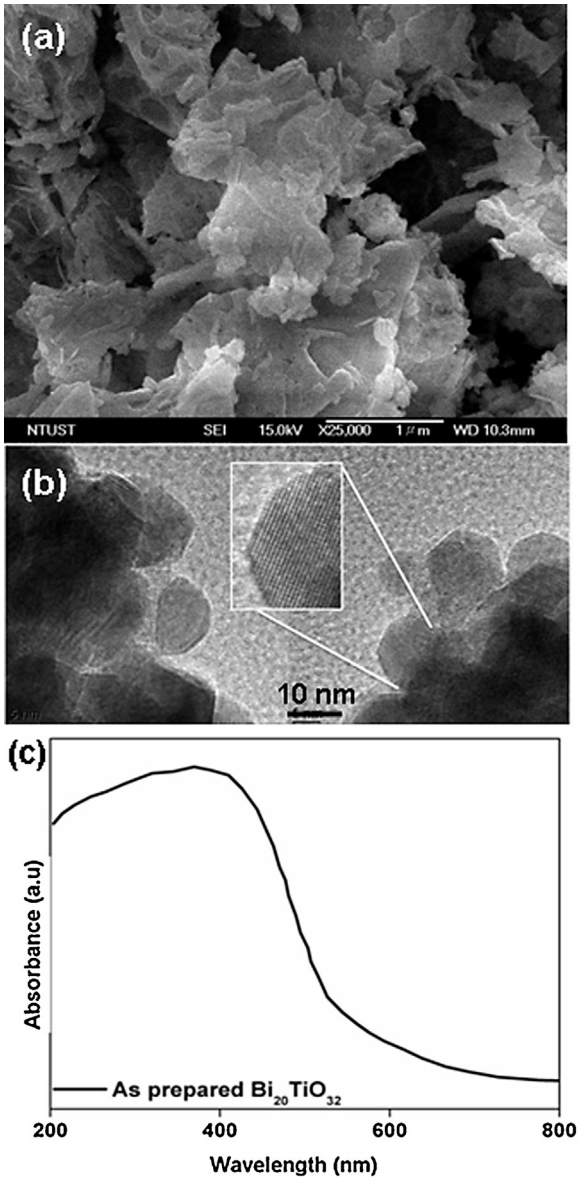

Fig. 4. The SEM (a) TEM (b) images and UV–visible spectra (c) of the as prepared $Bi_{20}TiO_{32}$ using system 4 and calcinated at 375 °C.

the silver ions act as sacrificial agent to trap the photo-excited electron so that the recombination of the photo-excited electrons with holes getting minimal. The photocatalytic activity of the as prepared $Bi_{20}TiO_{32}$ sample for water oxidation under UV–visible light illumination has been performed as shown in Fig. 5(a). The evolved gases as a result of photocatalytic reaction were detected by GC as seen in Fig. 5 (b). The result in our experiment shows that the activity increases at the beginning and then become saturated (Fig. 5(a)). As shown in Fig. 5(b), the oxygen peak is much more dominant than nitrogen peak. However, nitrogen peak still observed in this study may be caused by the incomplete gas evacuation during reactor vacuuming process along with some gas contamination during sample injection in gas chromatography.

The photocatalytic activity of the as prepared $Bi_{20}TiO_{32}$ with respect to different grain size for water oxidation was studied. As shown in Fig. 6, the photocatalytic activity of the as prepared sample decreases with increasing of grain size indicated that the crystallinity of the materials did not change significantly while the surface area reduces appreciably and affecting more to the photocatalytic activity of the as prepared $Bi_{20}TiO_{32}$. As aforementioned,

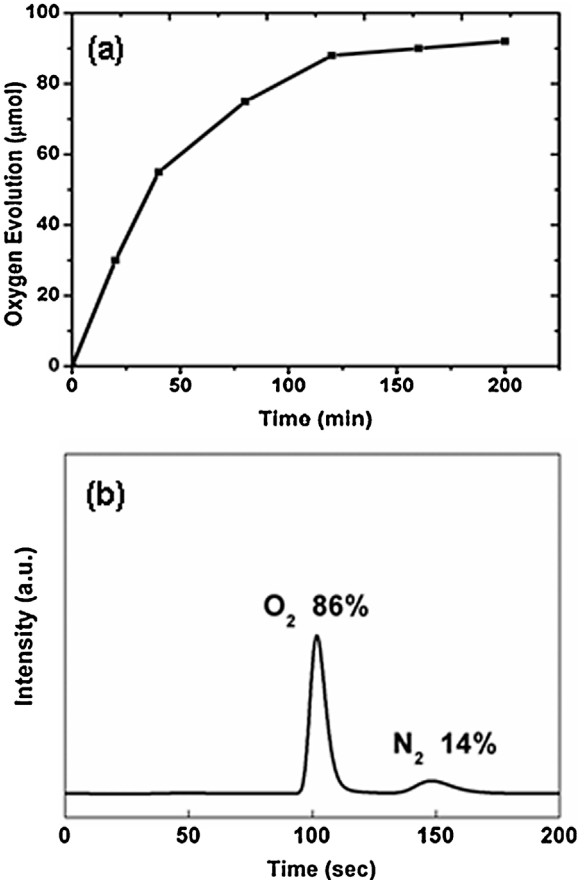

Fig. 5. The photocatalytic oxygen evolution of the as prepared $Bi_{20}TiO_{32}$ under UV–visible light illumination in 10 mM $AgNO_3$ solution (a) with gas chromatography profile of gases evolved from vacuum reactor during photocatalytic oxygen evolution reaction (b).

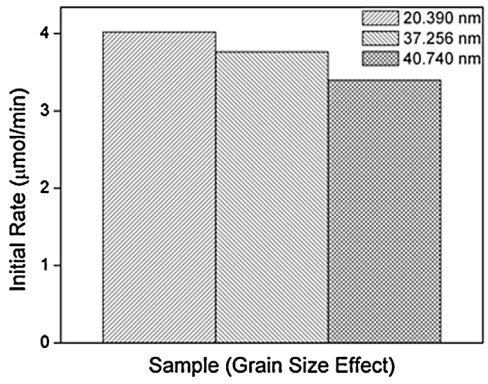

Fig. 6. Photocatalytic activity of $Bi_{20}TiO_{32}$ for oxygen evolution with respect to different grain sizes obtained from different ratios of citric acid to total metal ions (in 10 mM $AgNO_3$ solution).

different grain sizes of $Bi_{20}TiO_{32}$ were obtained at different ratios of citric acid to total metal ions. Increasing citric acid to metal ion ratio resulted in an increased grain size. Although the photocatalytic activity of the as prepared $Bi_{20}TiO_{32}$ is increasing by reducing the citric acid ratio to the metal ions, further decreasing of citric acid content cannot produce pure phase of $Bi_{20}TiO_{32}$ since the chelating agent is not enough to form a stable and good complex during sol–gel preparation. $Bi_{20}TiO_{32}$ prepared by the citric acid to metal ion ratio of 1:1 was used in the following experiments, unless otherwise stated.

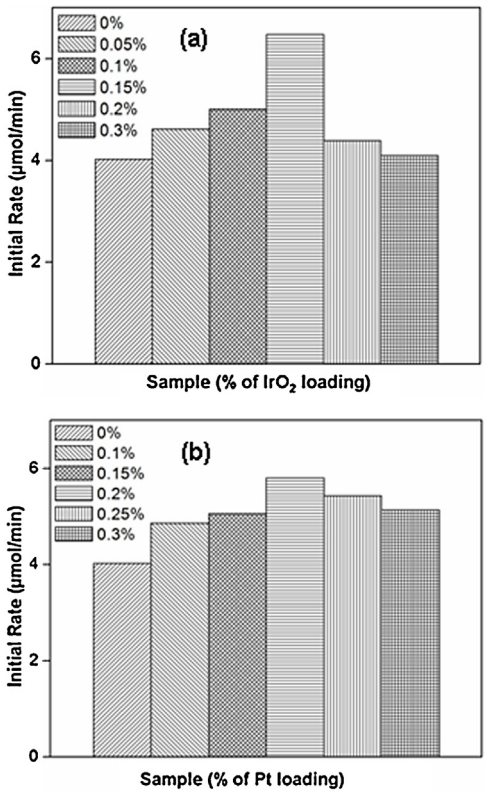

Fig. 7. Effect of iridium oxide (a) and platinum (b) co-catalyst loading on the initial oxygen evolution rate of the as prepared $Bi_{20}TiO_{32}$ photocatalyst (in 10 mM $AgNO_3$ solution).

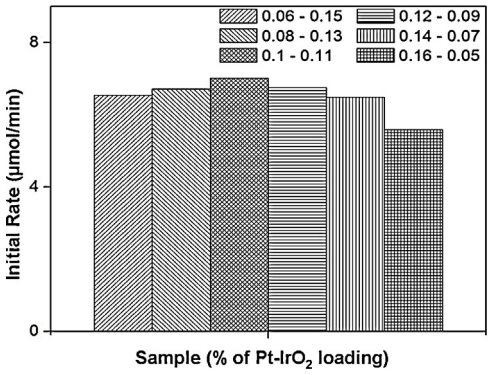

Fig. 8. Initial oxygen evolution rate at different wt% of platinum and iridium oxide co-catalyst (total of 0.21 wt %) loaded on $Bi_{20}TiO_{32}$ ($AgNO_3$, 10 mM).

The photocatalytic activity of oxygen evolution can be enhanced by introducing co-catalyst to the photocatalyst to reduce the photo-exited electron-hole recombination rate [35,36]. Iridium oxide is well known co-catalyst for water oxidation while platinum is usually chosen as electron trapper in hydrogen evolution photocatalyst [36]. Fig. 7 shows the initial oxygen evolution rate in comparison with different co-catalysts loading. The loading of iridium oxide reached its optimum value at 0.15 wt% (Fig. 7(a)) while platinum at 0.2 wt% (Fig. 7(b)) when they were loaded separately. Further increase of iridium oxide or platinum loading as showed in Fig. 7(a) and (b) decreased the initial oxygen evolution rate due to shielding effect of co-catalyst to the photocatalyst. The shielding effect of the photocatalyst may be also possible from the deposition of Ag after reduction (Fig. 9 (b)).

Further increase of the photocatalytic activity was achieved by combining iridium oxide and platinum co-catalyst as shown

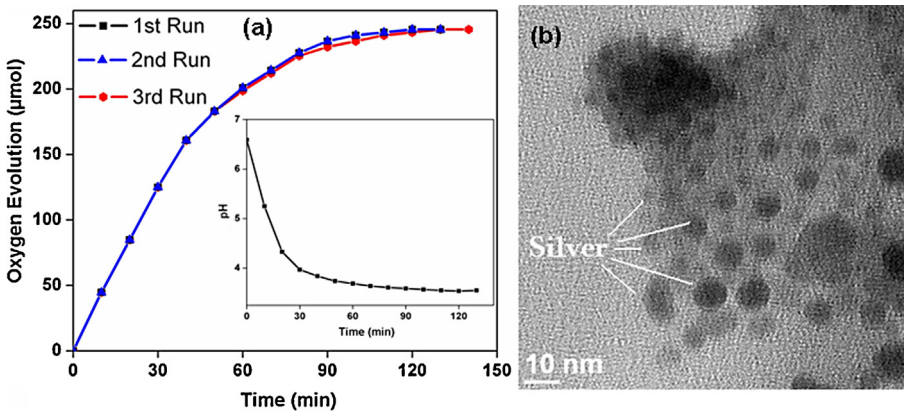

Fig. 9. Repeated tests of the as prepared $Bi_{20}TiO_{32}$ during photocatalytic oxygen evolution (a). The inset figure in (a) shows the changing pH during photocatalytic oxygen evolution; the TEM images of $Bi_{20}TiO_{32}$ (b) after the third run of photocatalytic test in aqueous solution of silver nitrate (10 mM $AgNO_3$ solution).

in Fig. 8. The total metal loading weight of platinum and iridium oxide was kept 0.21 wt% and various combination between two co-catalysts were applied. After several experiments using different amount of Pt-IrO_2 co catalysts conducted, the optimum coverage was found and the best combination of platinum loading was 0.1 wt% while iridium trioxide loading was 0.11 wt% (Fig. 8). The result in Fig. 8 indicates that the higher iridium oxide amount increases the photocatalytic activity more significantly as compared to the higher platinum amount; suggesting that the resistance for the water oxidation at the surface of iridium oxide is higher than that for photoexcited electron trapping process on Pt surface.

Effect of sacrificial agent concentration to the initial rate of photocatalytic oxygen evolution was studied for the as prepared $Bi_{20}TiO_{32}$ samples from citric acid to metal ion ratio of 1:1. The initial oxygen evolution rate in aqueous silver nitrate solution in the range of 0–25 mM increases linearly with increasing the concentration of silver nitrate, as seen in Fig. S1 (Supporting information). This suggests higher driving force for photo excited electron transfer from photocatalyst particle to sacrificial agent. This reduces the recombination of photo excited holes and electrons.

Finally, the reproducibility of oxygen evolution and the effect of pH on the photocatalytic activity of the as prepared sample were studied. Fig. 9(a) shows the photocatalytic activity result of the as prepared $Bi_{20}TiO_{32}$ sample carried out for three times. The oxygen evolution reaches maximum value after 2 h photocatalytic activity test. The pH value was monitored during photocatalytic activity test as shown in the inset figure in Fig. 9(a) with 10 min interval light illumination and gas collection. During photocatalytic activity test, pH value of the solution gradually decreased as the consequence of water oxidation and it can be seen as an indicator of reaction rate for water oxidation. The as prepared $Bi_{20}TiO_{32}$ photocatalyst with the best setup and configuration showed for initial oxygen evolution rate around 6 μmol/min under visible light illumination. The as prepared $Bi_{20}TiO_{32}$ photocatalyst was repeatedly tested for oxygen evolution and has good reproducibility as observed in Fig. 9(a). It is clearly seen that the activity of $Bi_{20}TiO_{32}$ was stable throughout three experimental runs with only a slight decrease at the end of the third run which resulted from the accumulation of silver nanoparticles on the surface of photocatalyst as shown in the TEM image in Fig. 9(b).

4. Conclusion

Pure $Bi_{20}TiO_{32}$ for oxygen evolution photocatalyst has been successfully synthesized by a sol–gel method using different precursor's combinations at low temperature. Based on the TGA profile of each precursor's combinations, 375 and 575 °C were chosen for calcinations. Among different combinations of starting materials, a pure phase $Bi_{20}TiO_{32}$ was obtained from a precursor compositions of bismuth nitrate–titanium isopropoxide–citric acid after calcinations at 375 °C temperatures. The effect of chelating agent to metal ions ratio on the synthesis of pure $Bi_{20}TiO_{32}$ in particular on grain size was studied and the lower grain size was obtained at 1:1 chelating agent to metal ions ratio. The photocatalytic activities of the as prepared $Bi_{20}TiO_{32}$ for oxygen evolution using silver nitrate as sacrificial agent under UV–visible light irradiation have been studied. The photocatalytic activity of the as prepared $Bi_{20}TiO_{32}$ was further enhanced by the addition of co-catalysts (iridium oxide and platinum). The highest photocatalytic activity of the as prepared $Bi_{20}TiO_{32}$ was shown with the combination of platinum and iridium oxide loading of 0.1 wt% and 0.11 wt% respectively. The as prepared $Bi_{20}TiO_{32}$ photocatalyst showed an initial oxygen evolution rate of 6 μmol/min under visible light illumination. The developed sol–gel method combining a chelating agent illustrates a simple and facile way to fabricate pure $Bi_{20}TiO_{32}$ which could not be fabricated easily due to their metastable structure under ambient condition. At the same time, it opens up a new approach to the synthesis of bismuth titanate-based photocatalysts for water oxidation and promising potential applications in z-scheme photocatalysis.

Acknowledgements

The financial supports from the National Science Council (NSC) (NSC-99-2120-M-011-001, NSC 99-2811-M-011-005, NSC 102-3113-P-011-001), and the Top University Projects of Ministry of Education (MOE) (102H451401), as well as the facilities supports from the National Synchrotron Radiation Research Center (NSRRC) and the National Taiwan University of Science and Technology (NTUST) are acknowledged.

Appendix A. Supplementary data

Supplementary data associated with this article can be found, in the online version, at http://dx.doi.org/10.1016/j.apcatb.2013.12.033.

References

[1] A. Fujishima, K. Honda, Nature 37 (1972) 238.
[2] Z. Zou, J. Ye, K. Sayama, H. Arakawa, Nature 414 (2001) 625.
[3] F.E. Osterloh, Chem. Mater. 20 (2008) 35–54.
[4] A.K. Agegnehu, C.-J. Pan, J. Rick, J.-F. Lee, W.-N. Sub, B.-J. Hwang, J. Mater. Chem. 22 (2012) 13849–13854.

[5] H. Husin, H.-M. Chen, W.-N. Su, C.-J. Pan, W.-T. Chuang, H.-S. Sheu, B.-J. Hwang, Appl. Catal. B: Environ. 102 (2011) 343–351.
[6] H. Husin, W.-N. Su, H.-M. Chen, C.-J. Pan, S.-H. Chang, J. Rick, W.-T. Chuang, H.-S. Sheu, B.-J. Hwang, Green Chem. 13 (2011) 1745–1754.
[7] D. Yamasita, T. Takata, M. Hara, J.N. Kondo, K. Domen, Solid State Ionics 172 (2004) 591–595.
[8] K. Maeda, K. Domen, J. Phys. Chem. C 111 (2007) 7851–7861.
[9] M.H.V. Huynh, T.J. Meyer, Chem. Rev. 107 (2007) 5004–5064.
[10] B.S. Yeo, A.T. Bell, J. Am. Chem. Soc. 133 (2011) 5587–5593.
[11] M.W. Kanan, D.G. Nocera, Science 321 (2008) 1072–1075.
[12] X. Zong, Z. Xing, H. Yu, Z. Chen, F. Tang, J. Zou, G.Q. Lu, L. Wang, Chem. Commun. 47 (2011) 11742–11744.
[13] J.H. Park, S. Kim, A.J. Bard, Nano Lett. 6 (2006) 24–28.
[14] P. Chatchai, Y. Murakami, S.-y. Kishioka, A.Y. Nosaka, Y. Nosaka, Electrochim. Acta 54 (2009) 1147–1152.
[15] T.K. Townsend, E.M. Sabio, N.D. Browningb, F.E. Osterloh, Energy Environ. Sci. 4 (2011) 4270–4275.
[16] S.S.K. Ma, T. Hisatomi, K. Maeda, Y. Moriya, K. Domen, J. Am. Chem. Soc. 134 (2012) 19993–19996.
[17] Y. Cong, H.S. Park, H.X. Dang, F.-R.F. Fan, A.J. Bard, C.B. Mullins, Chem. Mater. 24 (2012) 579–586.
[18] J. Guo, Y. Li, S. Zhu, Z. Chen, Q. Liu, D. Zhang, W.-J. Moonc, D.-M. Songc, RSC Advances 2 (2012) 1356–1363.
[19] J. Su, L. Guo, N. Bao, C.A. Grimes, Nano Lett. 11 (2011) 1928–1933.
[20] W. Wei, Y. Dai, B. Huang, J. Phys. Chem. C 113 (2009) 5658–5663.
[21] J. Tang, Z. Zou, J. Ye, J. Phys. Chem. C 111 (2007) 12779–12785.
[22] W.-F. Su, Y.-T. Lu, Mater.Chem. Phys. 80 (2003) 632–637.
[23] W.F. Yao, H. Wang, X.H. Xu, J.T. Zhou, X.N. Yang, Y. Zhang, S.X. Shang, Appl. Catal. A: Gen. 259 (2004) 29–33.
[24] W.F. Yao, H. Wang, X.H. Xu, S.X. Shang, Y. Hou, Y. Zhang, M. Wang, Mater. Lett. 57 (2003) 1899–1902.
[25] W.F. Yao, H. Wang, X.H. Xu, X.F. Cheng, J. Huang, S.X. Shang, X.N. Yang, M. Wang, Appl. Catal. A: Gen. 243 (2003) 185–190.
[26] P. DuraÂn, F. Capel, C. Moure, M. Villegas, FernaÂ ndez, Â.F. Jose, Tartaj J.s., A.C. Caballero, J. Eur. Ceram. Soc. 21 (2001) 1–8.
[27] Y. Hou, M. Wang, X. Xu, H. Wang, S. Shang, D. Wang, W. Yao, J. Cryst. Growth 240 (2002) 489–494.
[28] Y. Hou, M. Wang, X.-H. Xu, D. Wang, H. Wang, J. Am. Ceram. Soc. 85 (2002) 3087–3089.
[29] H. Cheng, B. Huang, Y. Dai, X. Qin, X. Zhang, Z. Wang, M. Jiang, J. Solid State Chem. 182 (2009) 2274–2278.
[30] J. Taing, M.H. Cheng, J.C. Hemminger, ACS Nano 8 (2011) 6325–6333.
[31] H.T. Gomes, B.F. Machado, A.M.T. Silva, G. Dražić, J.L. Faria, Mater. Lett. 65 (2011) 966–969.
[32] R.S. Amin, A.A. Elzatahry, K.M. El-Khatib, M.E. Youssef, Int. J. Electrochem. Sci. 6 (2011) 4572–4580.
[33] W.-C. Li, M. Comotti, F. Schüth, J. Catal. 237 (2006) 190–196.
[34] V. Barlier, V.R. Bounor-Legare', G.L. Boiteux, Joël Davenas, D. Léonard, Appl. Surf. Sci. 254 (2008) 5408–5412.
[35] G.R. Bamwenda, H. Arakawa, Appl. Catal. A: Gen. 210 (2001) 181–191.
[36] S. Shen, S.S. Mao, Nanophoton 1 (2012) 31–50.